1-8-2022

Light-driven dynamics between calcification and production in functionally diverse coral reef calcifiers

Jennifer Mallon

Tyler Cyronak

Emily R. Hall

Anastazia T. Banaszak

Dan A. Exton

See next page for additional authors

Authors

Adrian M. Bass

University of Glasgow

LIMNOLOGY and OCEANOGRAPHY

ASLO

Limnol. Oceanogr. 9999, 2022, 1–16

doi: 10.1002/lno.12002

Light-driven dynamics between calcification and production in functionally diverse coral reef calcifiers

Jennifer Mallon [1,2*], **Tyler Cyronak** [3], **Emily R. Hall** [4], **Anastazia T. Banaszak** [2*], **Dan A. Exton** [5], **Adrian M. Bass** [1*]

[1]School of Geographical and Earth Sciences, University of Glasgow, Glasgow, Scotland
[2]Unidad Académica de Sistemas Arrecifales, Universidad Nacional Autónoma de México, Puerto Morelos, Mexico
[3]Department of Marine and Environmental Sciences, Halmos College of Natural Sciences and Oceanography, Nova Southeastern University, Dania Beach, Florida
[4]Ocean Acidification Program, Mote Marine Laboratory, Sarasota, Florida
[5]Operation Wallacea, Spilsby, Lincolnshire, UK

Abstract

Coral reef metabolism underpins ecosystem function and is defined by the processes of photosynthesis, respiration, calcification, and calcium carbonate dissolution. However, the relationships between these physiological processes at the organismal level and their interactions with light remain unclear. We examined metabolic rates across a range of photosynthesising calcifiers in the Caribbean: the scleractinian corals *Acropora cervicornis*, *Orbicella faveolata*, *Porites astreoides*, and *Siderastrea siderea*, and crustose coralline algae (CCA) under varying natural light conditions. Net photosynthesis and calcification showed a parabolic response to light across all species, with differences among massive corals, branching corals, and CCA that reflect their relative functional roles on the reef. At night, all organisms were net respiring, and most were net calcifying, although some incubations demonstrated instances of net calcium carbonate ($CaCO_3$) dissolution. Peak metabolic rates at light-saturation (maximum photosynthesis and calcification) and average dark rates (respiration and dark calcification) were positively correlated across species. Interspecies relationships among photosynthesis, respiration, and calcification indicate that calcification rates are linked to energy production at the organismal level in calcifying reef organisms. The species-specific ratios of net calcification to photosynthesis varied with light over a diurnal cycle. The dynamic nature of calcification/photosynthesis ratios over a diurnal cycle questions the use of this metric as an indicator for reef function and health at the ecosystem scale unless temporal variability is accounted for, and a new metric is proposed. The complex light-driven dynamics of metabolic processes in coral reef organisms indicate that a more comprehensive understanding of reef metabolism is needed for predicting the future impacts of global change.

Coral reefs are highly productive ecosystems that build some of the largest living structures on Earth. The services obtained from the coral reef ecosystem include coastal protection, habitat provision, fisheries, and tourism (Hoegh-Guldberg et al. 2019). These services ultimately rely on biogenic calcification; the process by which a diverse community of framework-building corals, crustose coralline algae (CCA), and other calcifying organisms contribute to the calcium carbonate ($CaCO_3$) reef structure. Global climate change threatens the survival of important framework-building coral species, primarily through increasing seawater temperature and ocean acidification, both of which have been shown to directly impede coral growth and negatively impact coral reef-dwelling organisms and ecosystems (Kleypas and Yates 2009; Comeau et al. 2013). Exposed $CaCO_3$ structures and sediments are vulnerable to dissolution exacerbated by ocean acidification (Cyronak et al. 2013; Eyre et al. 2014), and it is expected that reef structure could be lost at a pace faster than it is constructed in the near future (Eyre et al. 2018).

A positive relationship between photosynthesis and calcification has been observed across cellular, organismal, and community scales in coral reefs (Gattuso et al. 1999; Allemand et al. 2011). At the ecosystem scale, the balance of

*Correspondence: jmallon967@gmail.com, banaszak@cmarl.unam.mx, adrian.bass@glasgow.ac.uk

Additional Supporting Information may be found in the online version of this article.

photosynthesis, respiration, calcification, and dissolution, collectively known as coral reef metabolism, controls the coral reef carbon cycle (Albright et al. 2015; Cyronak et al. 2018). Net ecosystem calcification is defined as the rate of $CaCO_3$ precipitation offset by dissolution, while net ecosystem production is defined as the difference between photosynthesis and respiration (Smith and Kinsey 1978). Reef metabolism is often measured through changes in the carbonate chemistry of sea water as it flows over a coral reef ecosystem, which requires detailed knowledge of the local hydrodynamics (Marsh and Smith 1978). The ratio of net calcification to net production has been proposed as a proxy for monitoring reef function, which can be calculated from carbonate chemistry data (Cyronak et al. 2018; Takeshita et al. 2018). This metric provides useful insight into reef biogeochemistry as a simple, effective tool for monitoring change in coral reef metabolism over space and time (Cyronak et al. 2018). However, the success of the calcification/production ratio metric depends on a strong mechanistic understanding of how photosynthesis and calcification are linked from the organism to the ecosystem.

At the organismal level, connectivity between photosynthesis and calcification is reflected in the phenomena known as light-enhanced calcification, or the observation of increased calcification rates during the day compared to night (Goreau 1959; Gattuso et al. 1999). Research into the mechanisms behind light-enhanced calcification have not yet reached a consensus, and it is possible that more than one process is taking place for the different species and functional groups exhibiting light-enhanced calcification, for example, corals, calcifying algae, foraminifera (Cohen et al. 2016). One hypothesis is that higher rates of photosynthesis associated with optimal light conditions provide the coral with more energy for calcification (Chalker and Taylor 1975). Other studies show that metabolic CO_2 production through respiration is an important source of carbon for calcification (Furla et al. 2000). Another hypothesis is that photosynthesis influences carbonate chemistry equilibrium at the site of calcification through the uptake of CO_2, which enhances $CaCO_3$ precipitation (McConnaughey and Whelan 1997; Allison et al. 2014). However, it is important to note that calcification and photosynthesis take place in different tissue layers (Jokiel 1978). Cohen et al. (2016) demonstrated that calcification can be decoupled from photosynthesis by providing corals with different wavelengths of light, indicating that both processes are independently linked to sunlight. To make accurate predictions about the impact of climate change on coral reefs, we must understand the mechanistic relationships between calcification and photosynthesis at the organismal scale before we can fully understand their interactions at community or ecosystem scales (Edmunds et al. 2016).

Shifting benthic community compositions are expected to alter the metabolism and carbon cycle of coral reef ecosystems (Hughes et al. 2018). In the Caribbean, coral reefs historically built by the skeletal calcium carbonate of reef-building corals, primarily branching *Acropora* spp. and massive *Orbicella* spp., have experienced unprecedented losses of coral cover and proliferation of macroalgal cover in recent decades (Jackson et al. 2014; Toth et al. 2019). Contemporary coral populations have lower species diversity and are dominated by resilient, weedy corals, such as *Porites astreoides* (Green et al. 2008), which lack reef-building life-history traits (Darling et al. 2012). As a result of these phase shifts, rugosity and carbonate accretion rates in the Caribbean have decreased over the past decades (Perry and Alvarez-Filip 2018), impacting the maintenance of reef structure and habitat function (Muehllehner et al. 2016; Yates et al. 2017; Kuffner et al. 2019). Quantifying organismal metabolic rates and understanding the dynamic interactions between metabolic processes is critical for predicting the impact of changing coral reef ecosystems and the ecosystem services they provide.

In this study, we measured the metabolic rates of key Caribbean coral reef calcifiers to determine the interaction among photosynthesis, respiration, and calcification over natural diurnal light cycles. We provide a comparison between species with distinct ecological functions, chosen to reflect past and present species dominance: (1) branching, rapid-growth *Acropora cervicornis*; (2) framework-building *Orbicella faveolata*; (3) resilient, weedy *Porites astreoides*; (4) framework-building, stress-tolerant *Siderastrea siderea*; and (5) abundant, low-profile, crustose coralline algae (CCA). We compared differences in metabolism across these calcifying organisms over a natural diurnal light cycle and developed metabolism–irradiance curves to determine the relationships among photosynthesis, calcification, and irradiance at the organismal level.

Methods

Ex situ incubations of four species of scleractinian coral and two crustose coralline algae (CCA) were conducted in the Climate and Acidification Ocean Simulator outdoor experimental facility at the Mote Marine Laboratory, Elizabeth Moore International Center for Coral Reef Research and Restoration, Summerland Key, Florida, in October and November of 2019. The Climate and Acidification Ocean Simulator facility is supplied with 20-μm particle-filtered Atlantic seawater maintained by a dual heat exchanger system at $28.4^{\circ}C \pm 0.2^{\circ}C$ (mean $\pm$ SD) in 3800-liter header tanks. An automated controller system (Walchem W900) maintains ambient seawater at a pH of 8.04 ± 0.04.

Study organisms

Small colonies (mean surface area $13 \pm$ SD 3.54 cm^2) of *A. cervicornis* ($n = 6$), *O. faveolata* ($n = 12$), *P. astreoides* ($n = 12$), and *S. siderea* ($n = 12$) were randomly selected from the Mote Marine Laboratory land nursery of micro-fragmented corals (Fig. 1a–f; Supporting Information Table S1). While small encrusting fragments do not represent the morphologies of larger, older colonies in the wild, using similarly

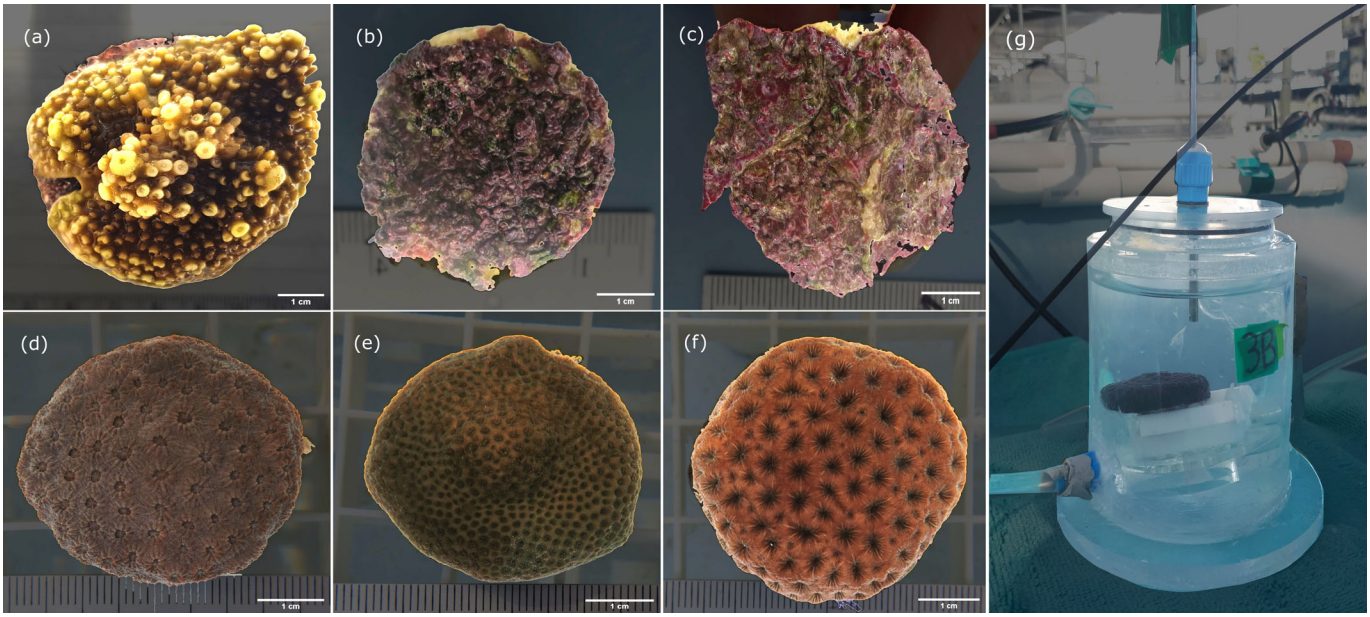

Fig 1. Examples of top-down photos used for surface area measurements on Image-J: (**a**) *Acropora cervicornis*, (**b**) crustose coralline algae type 1 (CCA1), (**c**) crustose coralline algae type 2 (CCA2), (**d**) *Orbicella faveolata*, (**e**) *Porites astreoides*, and (**f**) *Siderastrea siderea*, (**g**) the incubation chambers used during this study showing the oxygen sensor inserted through the chamber lid, transparent water jacket, and the white plastic holder below coral with stir bar spinning underneath. Photos (**a**) through (**f**) show 1 cm scale bars.

fragmented corals with minimal differences in "colony-wide" morphologies allows for better interspecific comparisons. All corals originated from Mote's restoration nurseries, where they had been either sexually produced and/or micro-fragmented from field-collected colonies between 2010 and 2017 (Supporting Information Table S2). In addition, crustose coralline algae growing on the base of two of the Mote restoration raceways were chiseled off and glued to clean ceramic tiles 3 weeks prior to the study. Due to morphological differences in color and surface texture (Fig. 1), CCA were thought to be distinct species; however, we were unable to identify them and are herein referred to as CCA type 1 (CCA1) and CCA type 2 (CCA2).

Each specimen was randomly assigned to one of 12 holding tanks (19-liter volume, 40 × 20 × 25 cm, $L \times W \times H$) 2 weeks prior to the study. Each tank received 160 mL min^{-1} filtered natural seawater via a separate manifold and each tank was fitted with a circulation pump to maintain flow (Deluxe Submersible Water Pump 400GPH). While water flow has been shown to modulate coral metabolism and their response to environmental change (Comeau et al. 2014, 2019), the goal of this study was to maintain a constant flow to compare the metabolism between calcifying functional groups. Sea water parameters of pH (Seven2Go Pro S8, Mettler Toledo), temperature, and salinity (YSI Professional Plus) were monitored twice per day. For pH, electrodes were calibrated against National Bureau of Standards scale buffers of 4.01, 7.00, and 10.00 at 25°C and validated using other carbonate chemistry parameters (e.g., total alkalinity [TA] and dissolved inorganic carbon [DIC]). Water temperature was controlled by an automated dual exchange heater and chiller, and, to maintain pH and salinity within each tank, water inflow was adjusted and changed as necessary. Supporting Information Table S3 provides an overview of the mean and standard deviation for all environmental parameters in the holding tanks. A permanent shade cloth (30% attenuation) maintained natural light conditions (daytime = 321.38 ± 179.73, μmol m^{-2} s^{-1}, and peak = 494 ± 64.4 μmol m^{-2} s^{-1} photosynthetically active radiation [PAR] mean ± SD). The surface area of each fragment was measured from top-down photos, with additional cylinder calculations to incorporate the surface area of *A. cervicornis* branches. All size measurements were extracted from photos using Image-J (Schneider et al. 2012) with the Simple Interactive Object Extraction plug-in (Wang 2016) to identify live tissue cover and exclude any areas of cement plug not covered in tissue (Fig. 1; Supporting Information Table S1).

Incubation protocol

Incubations were conducted over 12 d between 31 October 2019 and 21 November 2019, with each day selected for consistency in wind, cloud cover, and rainfall. One fragment per species was randomly selected each day and placed into an incubation chamber for ~ 1 h at the following times: 2 h after sunrise (AM), during the solar peak (PEAK), and 2 h after sunset (DARK). On 3 of the 12 d, an additional incubation between the solar peak and the sunset was included (PM). Separate readings of PAR were taken for each chamber position at

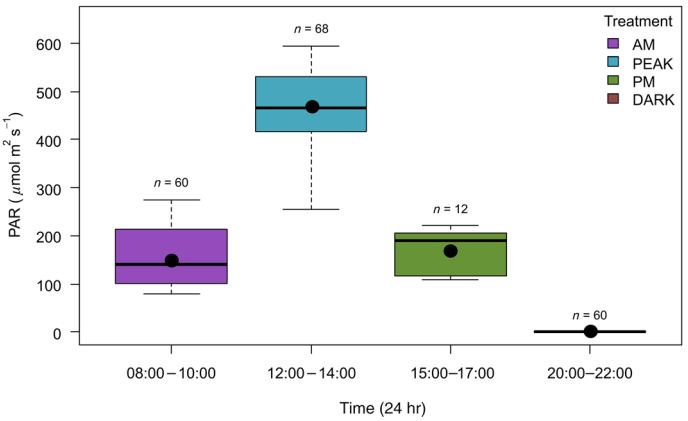

Fig 2. PAR measured during the different incubation time periods. Boxplots show mean (circle), median (horizonal line), and IQR (box and whisker). The number of individual incubations carried out within each time period (*n*) including control incubations is shown above each box. Colors represent the time periods: AM (2 h after sunrise 8 : 00 to 10 : 00), PEAK (solar noon 12 : 00 to 14 : 00), PM (2 h before sunset 15 : 00 to 17 : 00) and DARK (2 h after sunset 20 : 00 to 22 : 00). Average AM PAR was 155 ± 66.8 μmol m^{-2} s^{-1} (mean ± SD), PEAK 494 ± 64.4 μmol m^{-2} s^{-1}, and PM 171 ± 43.9 μmol m^{-2} s^{-1} PAR.

the start and end of incubations with Li-cor model LI-1500G and an underwater quantum sensor (LI-192SA), oriented horizontally. Average PAR light values (mean of start and end) were calculated for individual chambers and varied from 67 to 595 μmol m^{-2} s^{-2} between the three daylight incubation periods (8:00–10:00, 12:00–14:00, and 15:00–17:00; Fig. 2).

Incubation chambers were set up in a dry raceway tank adjacent to holding tanks for consistent light conditions. Incubations consisted of four double-walled transparent acrylic incubation chambers (300 mL) sealed with a transparent acrylic lid, with a rubber O-ring closure (Fig. 1g). A thermocycler (VWR MX7LR-20) recirculated water through the transparent cooling jackets of the incubators at 26.5°C ± 0.5°C to maintain water inside the chambers at 27.6°C ± 1.5°C. Incubation chambers were positioned on magnetic stirrers set at 600 revolutions per minute and flow simulated using a 2-cm stir bar placed under the specimens with a plastic grid base to allow water movement without disturbing the organism. All incubations were run for 1 h ± 3 min, with seawater samples taken at the start and end (see below for details).

Environmental parameters

Dissolved oxygen (DO) fiber-optic oxygen sensors (Firesting O_2, Pyroscience) were inserted in each chamber to ~ 1 cm above the coral 3–5 min prior to the incubation start time, to allow for acclimation of the sensor and adjustment of its position. The oxygen sensors were calibrated to 0% and 100% O_2 saturation using air-saturated water prior to each incubation. Real-time measurements of DO (μmol l^{-1}) were recorded each second during the incubation. To calculate oxygen fluxes, start and end values were calculated as the mean values over the first and last minute of the 1-h incubations. The fluxes derived from the start and end values were similar to fluxes derived from linear slopes between time and DO during each incubation (Supporting Information Figs. S1–S6). Start and end fluxes were used for a more direct comparison to fluxes derived from the carbonate chemistry data.

Water samples for carbonate chemistry analysis were taken at the start and end of incubations using a 100-mL plastic syringe; immediately filtered (0.45 μm), poisoned with 200 μL of saturated mercuric chloride, and stored in 250-mL amber borosilicate glass bottles at the Mote Ocean Acidification Laboratory until they were processed. One sample was collected at the start as all chambers were filled with the same water prior to beginning the incubations. TA was measured by potentiometric titration using an automated titrator (Metrohm 905 Titrando), following the standard best practice (Dickson et al. 2007). Mean values for each sample were derived from two to three samples (40 mL) with a precision of ± 3.8 μmol kg^{-1}. Measurements were corrected to Dickson Certified Reference Material (Batches 184, 187, and 189) measured at the start and end of each day. DIC was analyzed using an Apollo SciTech Analyzer (Model AS-C3). Mean values were derived from two to three replicates of 1 mL injections and corrected for drift with measurements of certified reference material at the start and end of the analysis. Precision of DIC measurements was 2.4 μmol kg^{-1}.

Calculations of metabolic processes

Metabolic rates were calculated from the difference between measurements taken at the end of the incubation minus the starting values (end – start) of DO (ΔDO), TA (ΔTA), and DIC (ΔDIC) concentrations. To calculate fluxes, all seawater chemistry measurements were normalized to individual incubation chamber volumes (259.69 ± 12.57 mL, mean ± SD) and coral surface areas (Supporting Information Table S1). Control incubations (e.g., empty ceramic tiles) showed negligible changes in seawater chemistry (ΔDO = 0.4 ± 6.8 μmol l^{-1}, ΔDIC = −7.2 ± 11.0 μmol kg^{-1}, ΔTA = −2.8 ± 8.7 μmol kg^{-1}, mean ± SD), and as such no corrections in seawater chemistry due to water column processes were made.

Net production (μmol cm^{-2} h^{-1}) for light incubations was calculated from changes in DO (P_{DO}) and DIC (P_{DIC}) concentrations according to the following equations:

$$P_{DO} = \frac{\Delta DO \times V}{A \times t} \quad (1)$$

$$P_{DIC} = -\frac{\left(\Delta DIC - \frac{\Delta TA}{2}\right) \times V}{A \times t} \quad (2)$$

where ΔDO, ΔDIC, and ΔTA represent the respective changes in DO, DIC, and TA concentrations in μmol L^{-1}. The volume of the incubation chamber in liters is represented as *V*, while

A is the surface area of the sample (cm^2), and t is duration of the incubation in hours (1 h). To calculate respiration (R_{DO} and R_{DIC}), the same equations were used with dark incubation data.

Net calcification (G_{net}) for light incubations was calculated using the alkalinity anomaly technique according to the following equation:

$$G_{net} = \frac{\left(-\frac{\Delta TA}{2}\right) \times V}{A \times t} \quad (3)$$

For dark calcification rates (G_{dark}) the same equation was used with data collected from dark incubations only.

The relationship between light and photosynthesis and calcification was modeled using gross metabolic rates (i.e., photosynthesis + respiration and calcification + dark calcification) using the following hyperbolic tangent function from Jassby and Platt (1976):

$$P_{net} = P_{max} \times \tanh\left(\frac{\alpha \times E}{P_{max}}\right) + R, \quad (4)$$

where P_{net} is the modeled net production rate, R is the average dark respiration rate, and E is the irradiance ($\mu mol\ m^{-2}\ s^{-1}$). The coefficients derived from the model include: the initial slope between P_{net} and light (α) and the maximum gross photosynthetic rate (P_{max}).

For calcification, we adapted Eq. 4 to model calcification (G_{net}) as:

$$G_{net} = G_{max} \times \tanh\left(\frac{\alpha \times E}{G_{max}}\right) + G_{dark} \quad (5)$$

where G_{dark} is the average dark calcification rate for each species, representing the non-light-enhanced portion of the measured calcification rates, G_{max} is the maximum gross calcification, and alpha (α) is the initial slope between calcification and irradiance.

The light saturation point (E_K) was calculated from model coefficients P_{max} or G_{max} and alpha for each model using the following equation:

$$E_K = \frac{P_{max}}{\alpha} \quad (6)$$

The absolute ratio of calcification to both calcification and production was calculated as follows:

$$G_{net}/M_{tot} = \frac{|G_{net}|}{|P_{net}| + |G_{net}|}$$

where M_{tot} (or the sum of both calcification and production) represents total carbon metabolism (*see* Discussion section for more details about this metric).

Statistical analysis

All statistical analyses were conducted in the statistical environment R using RStudio version R.4.0.2 (R Core Team, 2020). The *RespR* package (Harianto et al. 2019) was used to extract and inspect oxygen data (Supporting Information Figs. S1–S6). The *Tidyverse* (Wickham 2019) was used for data organization and synthesis, and data visualization was conducted with base-R functions and *ggplot/ggpubr* (Wickham 2016). Shapiro–Wilkes tests were combined with visual assessments of density and Q–Q plots to evaluate approximately normal distributions for individual species. Repeated measures two-way ANOVA tests were used to test differences between treatments and pairwise comparisons. Post hoc Bonferroni-corrected t tests were used to compare differences between all possible pairs of species at each time of day and for each parameter. Models were fitted using R linear and nonlinear least squares functions of the *Stats* package. Model fit was assessed by residuals plots generated using the *nlstools* package (Baty et al. 2015). Models were evaluated based on R^2, confidence intervals, and standard error of the regression (sigma, σ).

Results

Rates of metabolism were statistically different between treatment times for photosynthesis (repeated measures ANOVA for P_{DO} $F_{3,155} = 336.05$, $p = < 0.05$, and P_{DIC} $F_{3,143} = 331.37$, $p = < 0.05$), and for calcification (G_{net} repeated measures ANOVA $F_{3,149} = 27.24$, $p = < 0.05$) (Supporting Information Table S4; Fig. S7). During the day, photosynthesis ($+P_{DO}$ and $+P_{DIC}$) and calcification ($+G_{net}$) occurred in all incubations (Fig. 2). At night, respiration occurred in all incubations ($-P_{DO}$ and $-P_{DIC}$) while calcification was still generally positive ($+G_{net}$), although some net dissolution ($-G_{net}$) was detected (Fig. 3). Metabolic rates for all species were highest during the peak treatment (Fig. 3).

Metabolism was species specific, with *O. faveolata*, *P. astreoides*, and *S. siderea* having the highest average rates of calcification and photosynthesis, while both types of CCA had the lowest (pairwise comparisons using t test; Supporting Information Table S5). As *O. faveolata*, *P. astreoides*, and *S. siderea* had consistently similar rates, we refer to this grouping as the "massive corals" herein. We report rates as mean ± SD unless otherwise indicated. Overall, metabolic rates were higher in the massive corals than both *A. cervicornis* and CCA over a diurnal cycle (Fig. 4). Night metabolism followed a similar grouping as the daytime measurements: respiration was greater in the massive corals ($R_{DO} = -0.75 \pm 0.23$ $\mu mol\ cm^{-2}\ h^{-1}$, $R_{DIC} = -0.85 \pm 0.35$ $\mu mol\ cm^{-2}\ h^{-1}$), than in *A. cervicornis* ($R_{DO} = -0.32 \pm 0.05$, $R_{DIC} = 0.38 \pm 0.08$ $\mu mol\ cm^{-2}\ h^{-1}$) and CCA ($R_{DO} = -0.31 \pm 0.14$ $\mu mol\ cm^{-2}\ h^{-1}$, $R_{DIC} = -0.42 \pm 19$ $\mu mol\ cm^{-2}\ h^{-1}$). Dark calcification (G_{dark}) was higher in the massive corals ($G_{dark} = 0.31 \pm 0.24$ $\mu mol\ cm^{-2}\ h^{-1}$) than *A. cervicornis* ($G_{dark} = 0.03 \pm 0.08$ $\mu mol\ cm^{-2}\ h^{-1}$) and CCA ($G_{dark} = 0.06 \pm 0.18$ $\mu mol\ cm^{-2}\ h^{-1}$); however, this difference

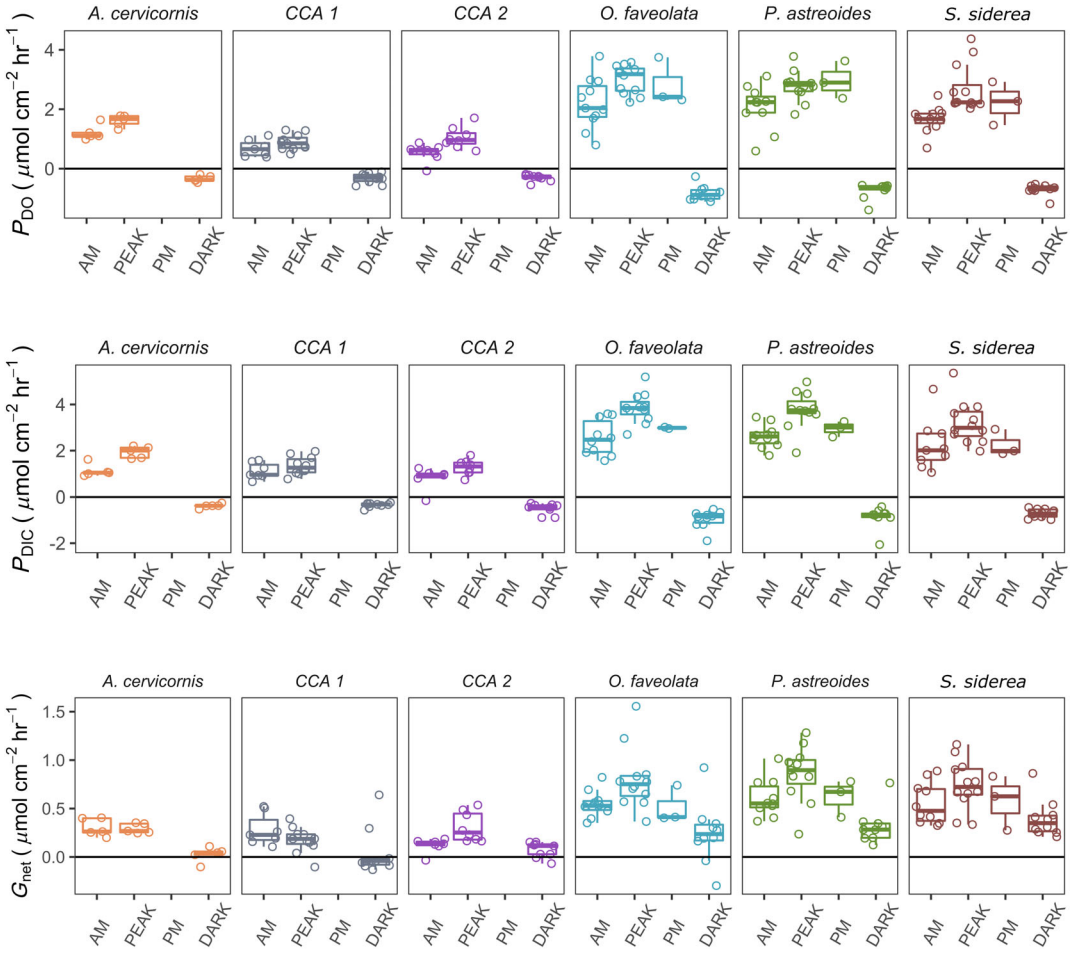

Fig 3. Boxplots of metabolic rates at different times of day for each species. *Y*-axes show; photosynthesis from oxygen evolution (P_{DO}), photosynthesis by carbon assimilation (P_{DIC}), and calcification (G_{net}) rates, normalized to time and surface area (fluxes in μmol cm^2 hr^{-1}). Boxplots show median (horizonal bar) and IQR (box and whisker), and individual data points are depicted as empty circles. Species are shown in colors and labeled above each plot. CCA1 and CCA2 are two types of crustose coralline algae. Time of day is shown on the *x*-axis: AM 08 : 00 to 10 : 00, PEAK 12 : 00 to 14 : 00, PM 15 : 00 to 17 : 00, and DARK 20 : 00 to 22 : 00. Only three species were incubated during the PM treatment.

was only significant for *S. siderea* (Supporting Information Table S5). Negative rates of dark calcification (i.e., $-G_{dark}$, net dissolution) were detected in 10 of the CCA, 1 of *A. cervicornis*, and 2 of *O. faveolata* dark incubations, although dissolution rates were relatively low and close to zero.

Relationships between metabolism and light

To elucidate species-specific relationships with light, metabolic–irradiance curves were modeled using a hyperbolic tangent equation (Eqs. 4, 5; Figs. 5, 6; Supporting Information Fig. S8). All photosynthesis–irradiance model evaluations had a high R^2 (> 0.80), and coefficients were significant ($p < 0.001$) for photosynthesis measured from changes to both DO (P_{DO}) and DIC (P_{DIC}). Calcification-light models generally had lower R^2 and higher sigma (σ) relative to calcification (G_{net}) values (Supporting Information Table S6) than photosynthesis–irradiance models, indicating a weaker model fit, and coefficient estimates were not always significant (alpha [α], $p > 0.1$ for *A. cervicornis* and crustose coralline algae). Of the coral species, *A. cervicornis* had the lowest maximum photosynthesis and calcification (P_{max} and G_{max}). The initial slope (α) of the photosynthesis–irradiance curves was highest for the massive corals. Photosynthetic–irradiance saturation (E_K) was highest in *A. cervicornis* (P_{DIC} $E_K = 356$), and in calcification–irradiance models light saturation (E_K) was highest for *P. astreoides* (G_{net} $E_K = 448$ μmol s^{-1} m^{-2}) and *S. siderea* (G_{net} $E_K = 544$ μmol s^{-1} m^{-2}).

Relationships between calcification and photosynthesis

The model coefficients P_{max} and G_{max} exhibited a positive linear relationship (Fig. 7) across all species ($R^2 = 0.88$, $p < 0.05$), while mean respiration (R) and dark calcification (G_{dark}) rates exhibited a negative linear correlation between all species ($R^2 = 0.66$, $p = 0.05$). This across-species relationship demonstrates that calcification increases with rates of net production during the day and with increased respiration in the

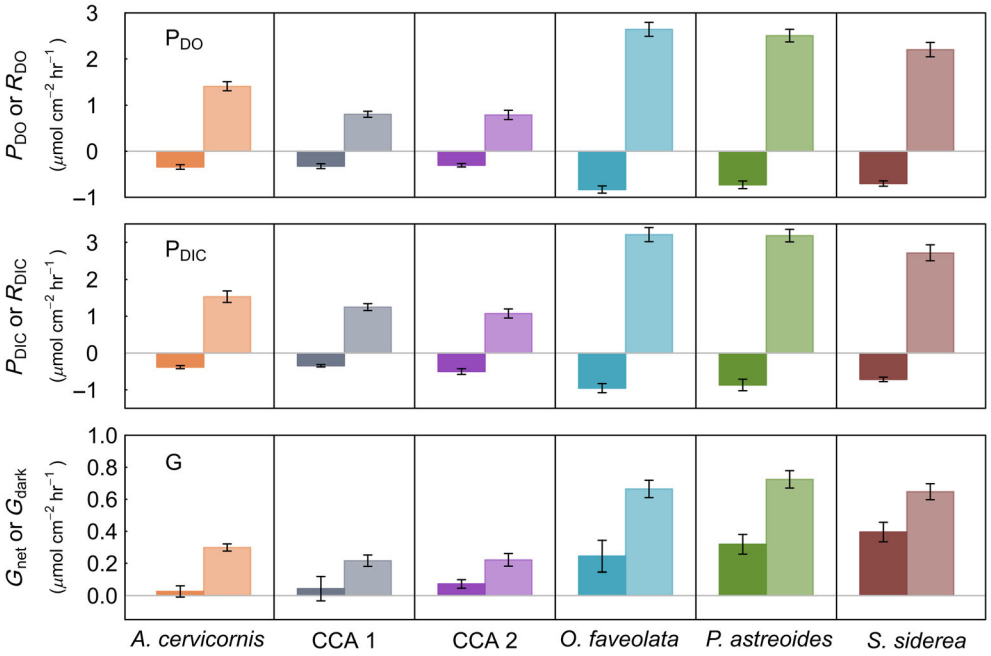

Fig 4. Paneled bar plots show species-specific average rates of dark (*left bar, darker shade*) and light (*right bar, lighter shade*) metabolism. Photosynthesis and respiration were calculated from both DO (P_{DO} and R_{DO}, *top*) and dissolved inorganic carbon (P_{DIC} and R_{DIC}, *middle*) fluxes. Light and dark calcification was calculated from changes in total alkalinity during light and dark incubations (G_{net} and G_{dark}, *bottom*). The color scheme is the same as in Fig. 3 and species are labeled on the bottom *x*-axis. CCA1 and CCA2 refer to the two types of crustose coralline algae used in this study. Rates shown are the mean light and dark rates across all days, and error bars represent standard error (SE).

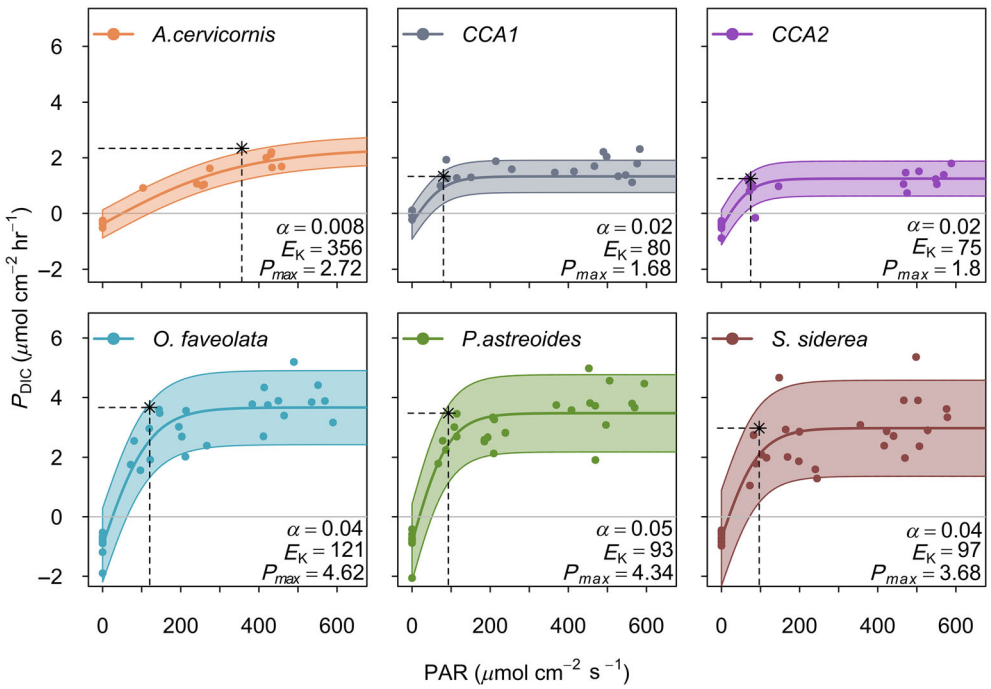

Fig 5. Photosynthesis–irradiance curves for *Acropora cervicornis*, crustose coralline algae (CCA1 and CCA2), *Orbicella faveolata*, *Porites astreoides*, and *Siderastrea siderea*, with photosynthesis measured from changes in dissolved inorganic carbon (P_{DIC}). Points show the measured net rates at distinct PAR light levels, and the solid, colored lines show the modeled metabolic curve. Shaded areas represent 95% confidence intervals. Dotted vertical lines indicate E_K (light saturation point) and dashed horizonal lines depict maximum net photosynthesis (P_{max} + R). Species-specific coefficients for the photosynthesis–irradiance models are displayed on each plot and full statistics provided in Supporting Information Table S6.

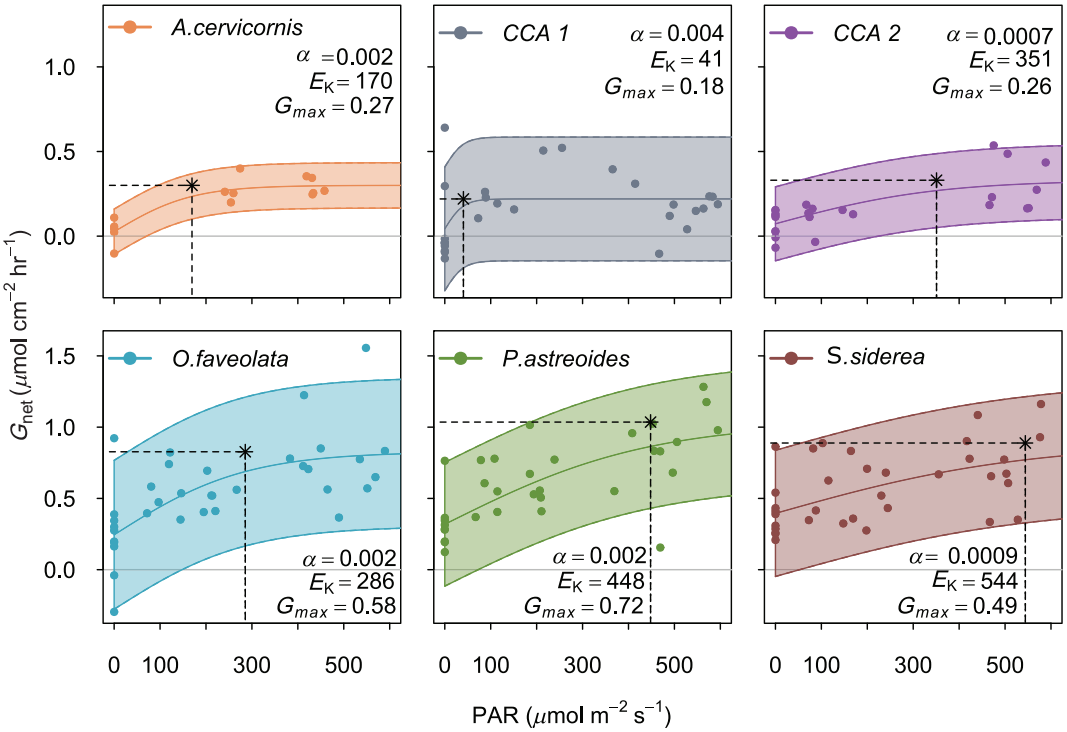

Fig 6. Species-specific calcification–irradiance models fitted to a hyperbolic tangent as described in the methods for *Acropora cervicornis*, crustose coralline algae (CCA1 and CCA2), *Orbicella faveolata*, *Porites astreoides*, and *Siderastrea siderea*. Shaded areas indicate the 95% confidence interval around the modeled curve. Modeled maximum net calcification ($G_{max} + G_{dark}$) and light saturation (E_k) points are depicted by dashed horizontal and vertical lines. Species-specific coefficients are displayed on each plot and full statistics provided in Supporting Information Table S6.

dark. When the metabolic rates of all species were grouped together, linear correlations between P_{DIC} and G_{net} were weaker (light $R^2 = 0.39$, $p < 0.001$, dark $R^2 = 0.15$, $p = 0.04$) than correlations between the model coefficients $G_{max} - P_{max}$ and $R - G_{dark}$ (Fig. 7c). When the linear models were broken down by species, regression models of P_{DIC} and G_{net} were only significant in *P. astreoides* (light $R^2 = 0.39$, dark $R^2 = 0.78$, $p < 0.005$; Fig. 8). These relationships indicate tight coupling of photosynthesis, respiration, and calcification, and show differences within and between different species of coral reef calcifiers.

DO production (P_{DO}) was positively correlated with DIC assimilation (P_{DIC}), indicating an overall metabolic quotient (Q) of 1.18 (Fig. 9a) with individual differences in Q between species (Fig. 9b; Supporting Information Table S7). The ratio of carbonate precipitation to organic production (G_{net}/M_{tot}) indicated that shifts in the balance of calcification to photosynthesis occur during the day in relation to irradiance (Fig. 10).

Discussion

This study aimed to determine the relationships among production, calcification, and light in a variety of calcifying coral reef organisms from the Caribbean. Differences were found in metabolism among morning, afternoon, and night incubations and were species specific; however, linearity between metabolic–irradiance model coefficients demonstrated that photosynthesis and calcification are correlated across species (Fig. 7). The results from this study confirm that photosynthesis and calcification rates of tropical benthic calcifiers exhibit a hyperbolic response to diurnal light cycles (Chalker and Taylor 1978; Cohen et al. 2016). Our analyses revisit the current understanding of relationships between organismal-level metabolism and irradiance in benthic coral reef calcifiers, and we interpret these findings in the context of ecosystem scale estimates of metabolism and predicted changes due to ongoing anthropogenic change.

Species-specific differences in metabolic rates

From the results of the incubations, three general groupings were apparent: (1) massive coral species *O. faveolata*, *P. astreoides*, and *S. siderea*; (2) *A. cervicornis*; and (3) crustose coralline algae. The highest metabolic rates were observed in massive coral species under all conditions (Figs. 3, 4). The metabolic rates of *A. cervicornis* and CCA were relatively similar, but they were grouped separately due to distinctions between the mechanisms by which coralline algae and corals calcify, and to reflect differences in the ecosystem function they provide. We discuss differences and similarities between the three groups in relation to their ecological function below.

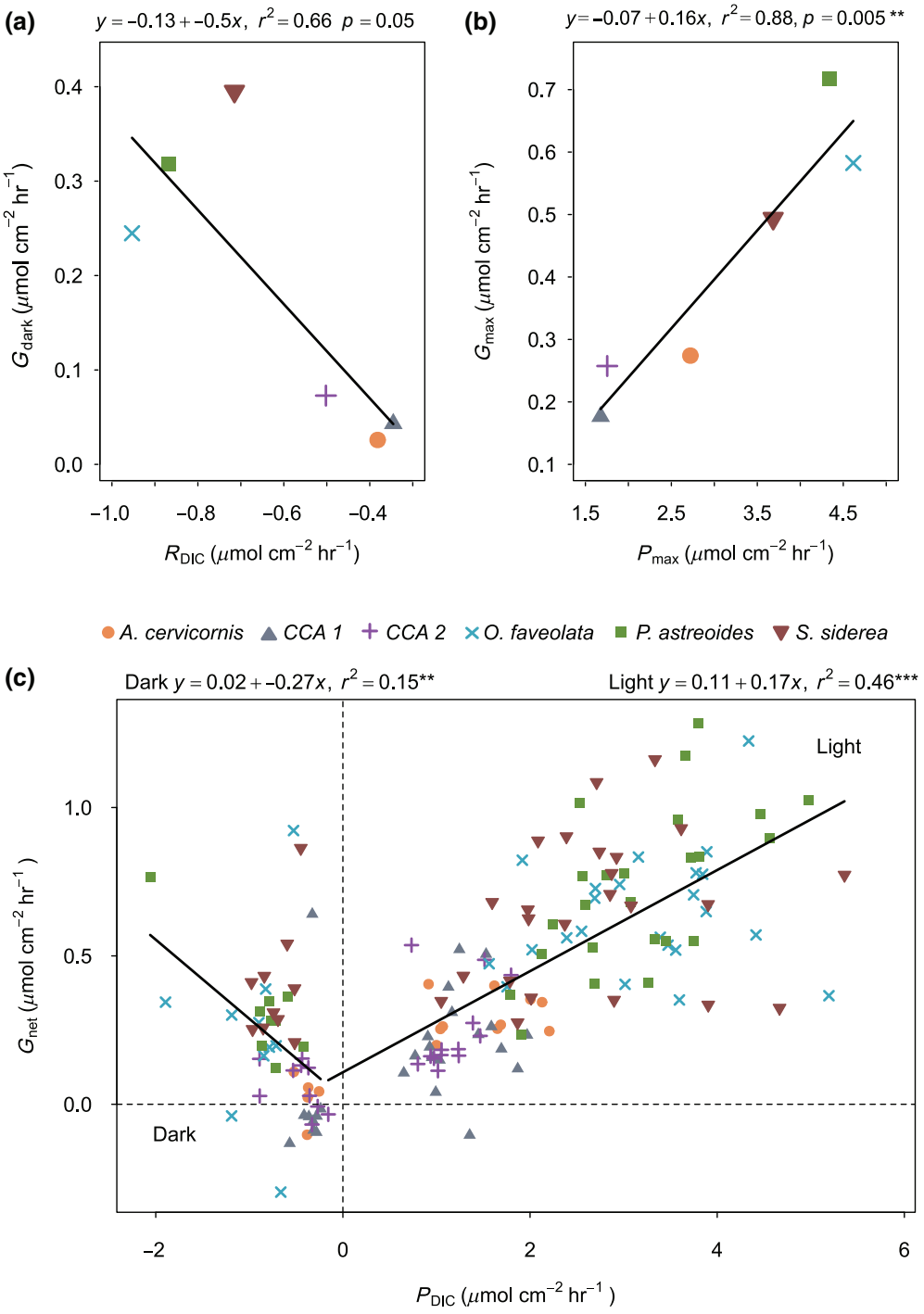

Fig 7. Linear relationships between (**a**) mean average respiration (R_{DIC}) and dark calcification (G_{dark}) for each species, (**b**) maximum metabolic rates derived from model coefficients for photosynthesis– and calcification–irradiance curves (P_{max} and G_{max}) and (**c**) individually measured photosynthesis (P_{DIC}) and calcification (G_{net}) rates. Individual species, *Acropora cervicornis*, crustose coralline algae (CCA1 and CCA2), *Orbicella faveolata*, *Porites astreoides*, and *Siderastrea siderea*, are depicted as different colors and symbols (*see* legend).

Metabolic rates were highest in the massive corals demonstrating that per area of live tissue, they produce more oxygen and calcium carbonate. Despite their higher metabolic rates, it is unlikely that massive corals have a stronger influence on community metabolism than branching *A. cervicornis* and encrusting CCA because of the relative benthic cover and architectural complexity of each species found in nature. Given the distinct ecological function and life-history traits within the massive coral grouping (Darling et al. 2012), the similarity in their metabolic rates was unexpected (Fig. 4). *P. astreoides* is

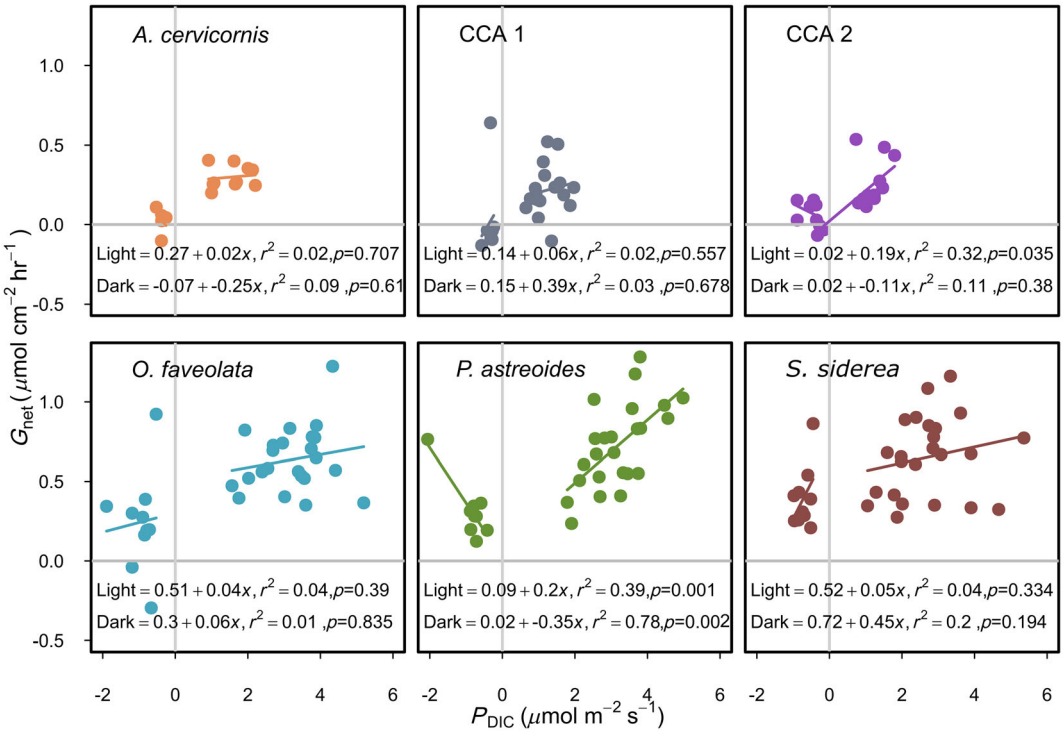

Fig 8. Linear relationships between photosynthesis (P_{DIC}) and calcification (G_{net}) for each species incubated in this study. CCA1 and CCA2 refer to crustose coralline algae types 1 and 2. Linear regression equations, R^2, and p values are displayed on each plot. Fitted regression lines are for dark (left-hand side of each plot) and light (right-hand side of each plot) incubations.

considered a weedy species of the Caribbean due to its fast growth, low-relief morphology, and ability to thrive in suboptimal conditions, whereas *O. faveolata* and *S. siderea* are key, framework-building corals (Darling et al. 2012). As Caribbean benthic communities undergo phase shifts, *P. astreoides* is colonizing space once dominated by massive, framework building corals to become one of the most abundant scleractinian corals on Caribbean coral reefs (Green et al. 2008). Our results show that the contribution of *P. astreoides* to community reef metabolism is at the same scale as that of traditional reef-building corals; however, the similarity in biogeochemical signal does not confer the same ecological traits, as *P. astreoides* does not provide habitat or architectural complexity to the reef (Green et al. 2008). Therefore, while shifts toward weedy species dominance may not be detectable via changes in reef metabolism, the changes in benthic composition will still impact reef carbon cycles and accretion through changes in calcium carbonate morphology and composition (Perry and Alvarez-Filip 2018). The third massive coral, *S. siderea*, is generally considered a slow-growing species. However, its calcification rates were also high, and the observed slow growth despite high calcification rates could be related to the high density of *S. siderea* skeletons (Hughes 1987).

Fast-growing *A. cervicornis* had the lowest calcification rates of the corals in this study, but they can also have relatively lower skeletal densities than the massive corals (Kuffner et al. 2017). Historically, *A. cervicornis* was a primary reef-building coral species and occupied more space on shallow water tropical reefs in the Caribbean than any other scleractinian coral (Rodríguez-Martínez et al. 2014; Toth et al. 2019); however, it and *Acropora palmata* have declined by over 80% over recent decades in the Caribbean (Jackson et al. 2014; Rodríguez-Martínez et al. 2014). It is possible that the lower rates of calcification observed in *A. cervicornis* were influenced by the relatively low flow induced within the mesocosm setting, as higher wave action may stimulate growth in this species (Jokiel 1978); however, our calcification rates agree with previous estimates (Chalker and Taylor 1975; Chalker and Taylor 1978). Colonies of *A. cervicornis* have a complex, branching structure with high surface area and they contribute different ecosystem functions compared to massive corals (Alvarez-Filip et al. 2011; Darling et al. 2012), which is reflected in the lower metabolic rates observed in our study. In general, *A. cervicornis* has low calcification yet high accretion rates, although skeletal density shows plasticity based on growing conditions (Kuffner et al. 2017). The life-history trait of lower density skeletons could promote asexual reproduction when high energy wave action fragments branches of larger colonies, allowing for the rapid proliferation of *Acropora* spp. (Tunnicliffe 1981; Lirman 2000). Despite having lower calcification rates than the massive corals, *A. cervicornis* provides a unique habitat for the biodiversity of species which reside in the dense thickets formed by this branching coral (Tunnicliffe 1981; Precht et al. 2002).

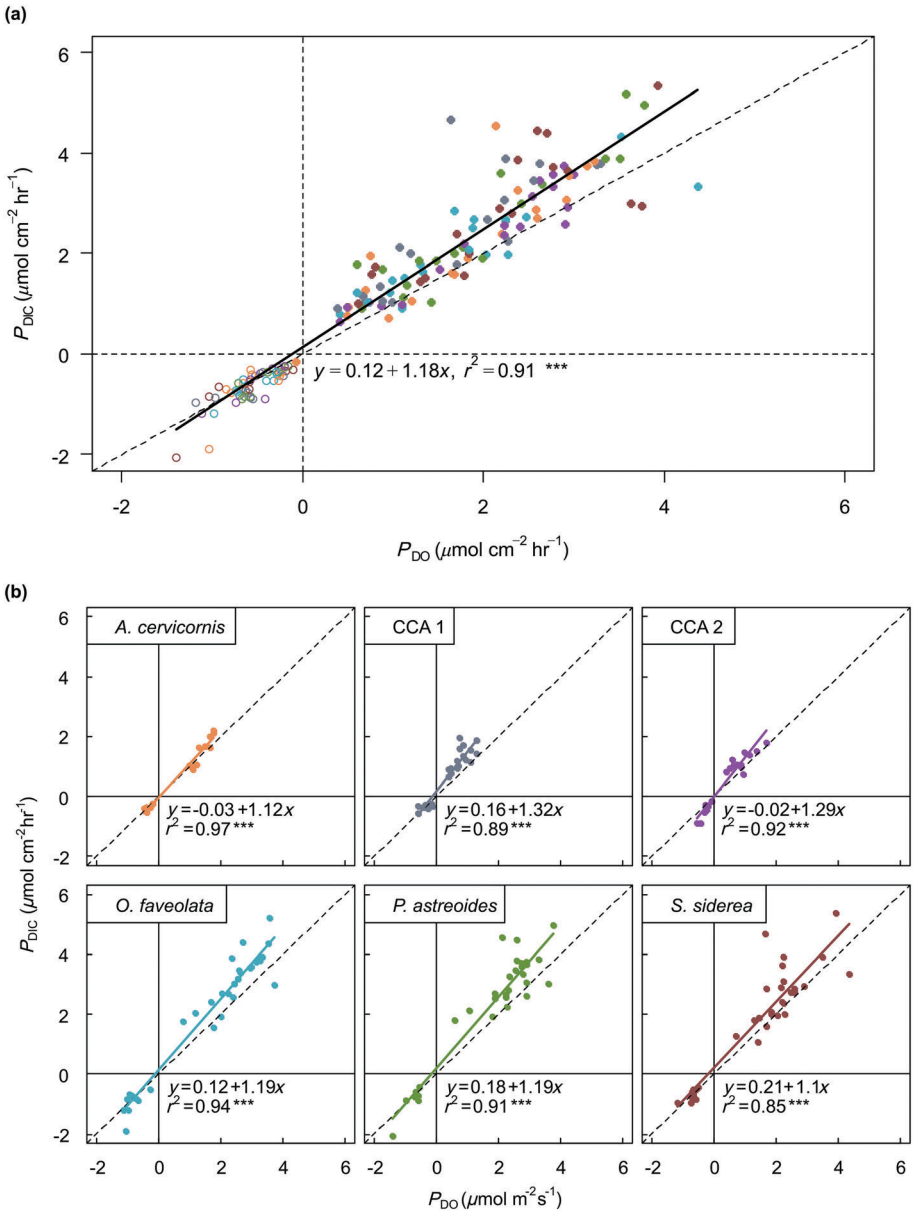

Fig 9. Linear models showing strong positive relationship between photosynthesis measured by carbon assimilation (P_{DIC}) and oxygen production (P_{DO}) (**a**) across species and functional groups, and (**b**) separated by species. All linear models were significant to the $p < 0.001$ level (denoted by ***). CCA1 and CCA2 refer to the two types of crustose coralline algae used in this study.

The lowest metabolic rates were recorded for crustose coralline algae; biogenic calcifiers which reinforce and strengthen the calcium carbonate matrix to cover otherwise exposed coral skeleton (Littler and Littler 2013). In addition, they promote calcification by scleractinian corals (Chisholm 2000) via inducing larval settlement and providing substrate for juvenile corals to grow (Heyward and Negri 1999). Due to their encrusting morphology, crustose coralline algae are often overlooked in quantification of coral reef calcification and accretion based on visual surveys. We report rates of calcification and photosynthesis in CCA in line with framework building *A. cervicornis* (Figs. 3, 4). This demonstrates the important contribution that crustose coralline algae can play in coral reef ecosystem metabolism beyond their other ecological functions. The two crustose coralline algal types were the closest to displaying net dissolution, indicating calcification slows or stops at night within this functional group, potentially due to dependence on light. Crustose coralline algae are expected to be more heavily impacted by ocean acidification than corals due to the higher proportion of high magnesium calcite in their skeletons, which could disproportionately impact the role of these organisms as important benthic calcifiers (Diaz-Pulido et al. 2012).

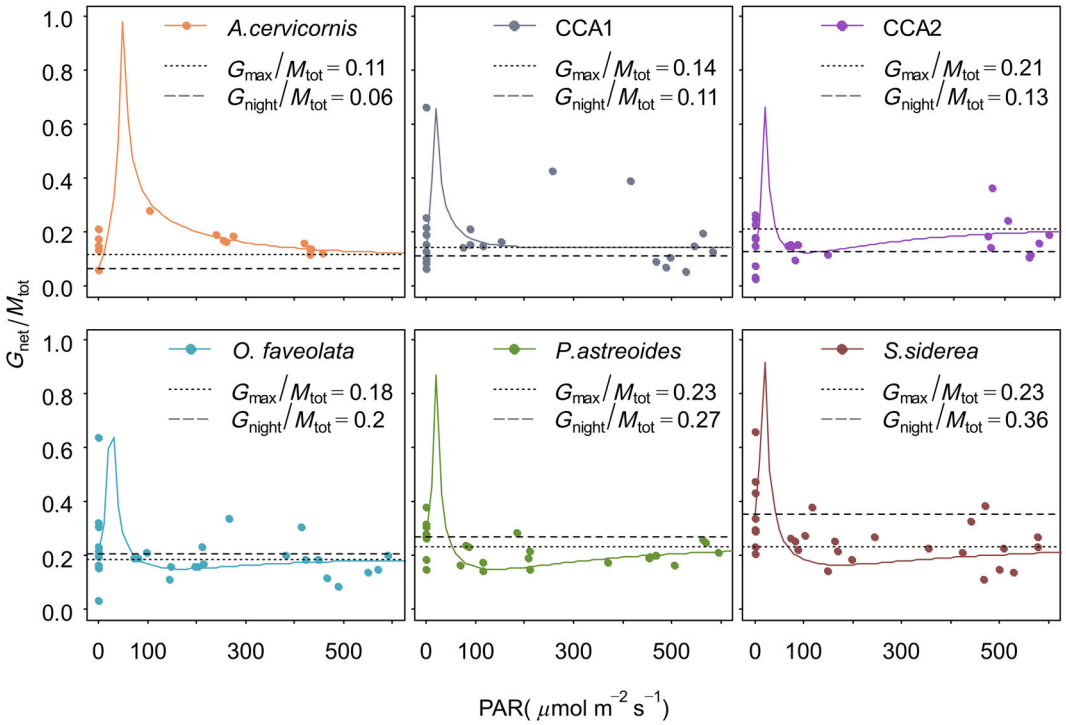

Fig 10. Ratios of calcification to total carbon metabolism (G_{net}/M_{tot}) calculated from each incubation (points) and metabolism–irradiance models (lines) plotted against PAR. Ratios calculated using the model coefficients (i.e., net P_{max} and netG_{max}; R and G_{night}) are depicted by dotted and dashed lines and values are displayed in the top right of the plot for each species. CCA1 and CCA2 refer to the two types of crustose coralline algae used in this study.

Impact of light on species-specific metabolism

Coral reefs encompass diverse and dynamic light environments over hourly, daily, and seasonal scales (Edmunds et al. 2018). However, most reef-wide estimates of community metabolism are conducted on timescales that do not incorporate instantaneous changes in light, even though community metabolism can change on sub-hourly timescales (Takeshita et al. 2016). Applying metabolic-light models to high-resolution time series of light could provide more complete estimates of community level metabolism. Studies have shown that scaling up to community and ecosystem levels from organismal studies can be complicated in coral reef ecosystems (Edmunds et al. 2016); however, the comparisons in our study add important insight into coral reef metabolism research. In this study, net metabolic rates (both photosynthesis and calcification) fit a commonly used hyperbolic function with light (Figs. 5, 6) (Jassby and Platt 1976), supporting the idea that both photosynthesis and calcification are driven by light (Falkowski et al. 1984; Cohen et al. 2016).

Photosynthesis–irradiance models fitted with both oxygen and carbon data sets (e.g., P_{DO} and P_{DIC}) demonstrated that photosynthetic efficiency (α), modeled maxima (P_{max}), and average respiration were greatest in the massive corals, highlighting that these species are drivers of coral reef production (Fig. 5; Supporting Information Fig. S8). Light saturation (E_K) was higher in *A. cervicornis* and CCA, potentially reflecting their ability to thrive in the shallowest and most sunlit areas of the reef (i.e., lagoon and crest). For calcification–irradiance models, the massive species group had the highest maximum and dark rates (G_{max} and G_{dark}), while estimates of calcification efficiency (α) were mixed across species. The differences between metabolic-light models support previous work showing that photosynthesis and calcification have species-specific and independent relationships with light (Gattuso et al. 2000; Sawall et al. 2018).

Relationships among photosynthesis, respiration, and calcification have been shown to exist across a wide range of marine calcifiers, and in the current study, we demonstrate that a strong relationship exists across different species, genera, and functional groups (Fig. 7). The strong positive linear relationship between G_{max} and P_{max} indicates that maximum net daytime photosynthesis and calcification rates are linked (Fig. 7b). We also found a strong negative linear relationship between average respiration and dark calcification across all species at night, indicating that dark calcification is linked to energy produced from respiration (Fig. 7a). Linear relationships also existed during the day and night for measured values of calcification and photosynthesis across all species (light $R^2 = 0.46$, $p < 0.0005$, dark $R^2 = 0.15$, $p = 0.005$; Fig. 7c). However, relationships between calcification and photosynthesis were less clear within each individual species (Fig. 8). This could be due to lower replicates within each

species and smaller ranges in dark rates that made it difficult to detect a clear relationship by species. While our study shows that photosynthesis and calcification are linked across benthic calcifiers, we also saw differences at the species level (Fig. 8), likely related to ecological function (González-Barrios and Álvarez-Filip 2018). For example, *P. astreoides* has a strong linear relationship between calcification and photosynthesis (light $R^2 = 0.39$, dark $R^2 = 0.78$, $p \leq 0.005$, Fig. 8), whereas other species such as *A. cervicornis* did not. Calcification of different species of corals has been shown to respond to global change differently (Kornder et al. 2018), which may reflect the interaction of these two processes at the cellular or organismal level. Light has also been shown to modulate the response of calcification to ocean acidification (Suggett et al. 2013). Therefore, developing species level metabolic irradiance curves under current and predicted ocean chemistry is important for understanding future impacts of global change.

The functional relationship among light, photosynthesis, and calcification is complex and operates at multiple levels (Allemand et al. 2011). We demonstrate a positive linear relationship between modeled metabolic maxima (G_{max} and P_{max}), indicating that energy from photosynthesis and respiration drive calcification. It is clear that coral metabolic processes are tightly coupled (Gattuso et al. 1999). However, recent research indicates that photosynthesis and calcification are parallel but independent light-driven processes (Cohen et al. 2016). The link between photosynthesis and calcification (i.e., light-enhanced calcification) at the organismal scale may be related to these processes co-evolving to occur at similar times due to increased energy supply for calcification (Sorek et al. 2014). If that is the case, then the relationships between photosynthesis and calcification found at the organismal level may not be as intimately linked within cells as previously thought. Further research is needed to define the functional relationships among light, photosynthesis, and calcification from the cell to the organism to better predict the impacts of global change on coral ecosystems.

Knowing instantaneous relationships between light and metabolism at the organismal scale (Figs. 5, 6; Supporting Information Fig. S8) could help scale metabolism rates up to the community and ecosystem at finer temporal scales. Direct measurements of coral reef net ecosystem metabolic rates are time consuming, expensive, and often require specific environmental conditions (Gattuso et al. 1999). Newer technology is being developed that can estimate community benthic metabolism rates over high-resolution temporal scales (< 1 h) using boundary layer techniques (i.e., eddy correlation and BEAMS) that measure oxygen and pH (Barnes and Devereux 1984; Long et al. 2013; Takeshita et al. 2016). These techniques require that we know the ratio of carbon and oxygen uptake and removal during the processes of photosynthesis and respiration (e.g., ΔDIC/ΔDO). For an organism, these values are usually seperated between day and night and known as the gross photosynthetic (PQ) and respiratory quotients (RQ), respectively. However, over daily cycles across organisms, communities, and ecosystems, the net metabolic quotient (*Q*) is needed for calculating metabolic rates from oxygen and pH measurements (Barnes and Devereux 1984; Takeshita et al. 2016). By measuring both oxygen and carbon fluxes, we were able to determine the net metabolic quotient for the different species in this study (Fig. 9). The net metabolic quotient (Q) was higher for crustose coralline algae (1.55 ± 0.49) than coral species (1.24 ± 0.38), which reflects elevated carbon assimilation compared to oxygen production. For corals, the metabolic quotient was similar across species (1.1–1.2), and closer to a 1 : 1 ratio, although the values still indicated a greater assimilation of carbon compared to DO production. Overall, the net metabolic quotient *(Q)* was 1.18 for all species and incubations combined. Interestingly, there was a trend of increasing Q with light when all corals were grouped together, indicating that the metabolic quotient may be more variable over short time scales than previously assumed (Supporting Information Fig. S10). Further understanding the influence of light on the balance of carbon assimilation to dissolved oxygen production will help to build our understanding of the reef net metabolic quotient and how it changes with light variability over hourly, daily, and seasonal cycles. More estimates of species-specific metabolic quotients for coral reef organisms will help in efforts aimed at using readily available pH and oxygen sensors to monitor the metabolism of coral communities at a greater resolution in both space and time.

Ratios of organic and inorganic carbon cycling in coral reef organisms

Ratios of net calcification to photosynthesis (G_{net}/P_{net}) quantify the relative balance between these two processes and have been proposed to be a useful metric for reef biogeochemical function and health (Cyronak et al. 2018). Previous studies have shown that G_{net} to P_{net} ratios range from −8 to 17 on the organismal scale and from 0 to 0.7 on an ecosystem scale (Gattuso et al. 1999; Cyronak et al. 2018). In this study, we calculated absolute ratios of net calcification to the sum of net calcification and net photosynthesis (G_{net}/M_{tot}) according to Eq. 7. We chose this metric because both calcification and production can be negative, which results in unreliable values as either the denominator or numerator approach 0. Also, we believe thatG_{net}/M_{tot} is more intuitive than G_{net}/P_{net} as it represents the relative proportion of total carbon metabolism due to calcification and ranges between 0 and 1. In all of the incubations, G_{net}/M_{tot} ranged from 0.03 to 0.66, which indicates that when both calcification and production are occurring production tends to dominate (Fig. 10). However, when the ratios were calculated using the metabolism–irradiance curves, G_{net}/M_{tot} ranged from 0 to 1 and all organisms exhibited a strong peak at the irradiance level where net photosynthesis crosses 0. This is because as net photosynthesis approaches 0 the absolute ratio comes closer to $|G_{net}|/|G_{net}|$. Ratios

calculated using the model coefficients for maximum calcification and photosynthesis (i.e., *net* G_{max} and *net* P_{max}) and night calcification to respiration (i.e., G_{dark} and R) ranged from 0.11 to 0.23 and 0.06 to 0.36, respectively (Fig. 10).

The light-induced changes in G_{net}/M_{tot} indicate that there is not one value that can readily describe the relative ratio of calcification and production for each calcifying organism, and that organisms can "equilibrate" to very different values during the day and night. In fact, the highly dynamic nature of G_{net}/M_{tot} related to light brings into question the use of G_{net} to P_{net} ratios as a single, determinant value of reef function and health at the ecosystem scale (Cyronak et al. 2018). If G_{net}/M_{tot} do not stabilize to one consistent value on an organismal scale, it is difficult to imagine that these ratios stabilize over varying light regimes across reef communities and ecosystems made up of many calcifying and non-calcifying organisms. Future work into determining the importance and usefulness of G_{net}/M_{tot} as a metric for reef biogeochemical cycling is needed.

Conclusions

We identified patterns in the metabolism of six Caribbean benthic calcifiers under natural diurnal light cycles. Our findings support previous work showing that photosynthesis and calcification are parallel processes driven by irradiance (Gattuso et al. 2000; Cohen et al. 2016), highlighting the importance of considering natural variations in light for all reef metabolism studies. Some metabolic rates of individual species could be generalized to larger categorical groupings such as the "massive coral" species. However, both *A. cervicornis* and crustose coralline algae had similar metabolic rates despite occupying very different functional niches in coral reef accretion. While calcification and photosynthesis both fit traditional hyperbolic tangent functions with light, coefficients of the metabolism–irradiance models varied between species. Interestingly, the modeled metabolic maxima (G_{max} and P_{max}) and dark calcification and respiration (G_{dark} and R) were correlated across all photosynthesising calcifiers in this study. These correlations support the idea that energy provided by photosynthesis and respiration may be an important control on organismal calcification across different calcifying functional groups. However, mechanistic studies are needed to further address this. Understanding the dynamic species-specific balance of calcification and production could provide useful insights into estimates of community- and reef-wide carbon cycles. For example, our results demonstrate that benthic surveys with simple groupings of calcifying and non-calcifying organisms could give important insights into coral reef carbon cycles. Finally, we established dynamic relationships between calcification and photosynthesis over diurnal light cycles that bring into question the application of calcification to photosynthesis ratios to monitor biogeochemical function on an ecosystem scale. Overall, the carbon cycle of coral reefs is highly dynamic at the organismal scale, driven by complex relationships between photosynthesis, respiration, calcification, and light. These relationships likely scale up and interact with other biogeochemical and hydrodynamic processes to create the intense variations in carbon chemistry observed on modern coral reefs.

References

Albright, R., J. Benthuysen, N. Cantin, K. Caldeira, and K. Anthony. 2015. Coral reef metabolism and carbon chemistry dynamics of a coral reef flat. Geophys. Res. Lett. **42**: 3980–3988. doi:10.1002/2015GL063488

Allemand, D., É. Tambutté, D. Zoccola, and S. Tambutté. 2011. Coral calcification, cells to reefs, p. 119–150. *In* Coral reefs: An ecosystem in transition. Springer.

Allison, N., and others. 2014. Corals concentrate dissolved inorganic carbon to facilitate calcification. Nat. Commun. **5**: 5741. doi:10.1038/ncomms6741

Alvarez-Filip, L., N. K. Dulvy, I. M. Côteé, A. R. Watkinson, and J. A. Gill. 2011. Coral identity underpins architectural complexity on Caribbean reefs. Ecol. Appl. **21**: 2223–2231. doi:10.1890/10-1563.1

Barnes, D. J., and M. J. Devereux. 1984. Productivity and calcification on a coral reef: A survey using pH and oxygen electrode techniques. J. Exp. Mar. Biol. Ecol. **79**: 213–231. doi:10.1016/0022-0981(84)90196-5

Baty, F., C. Ritz, S. Charles, M. Brutsche, M.-L. Flandrois, and J.-P. Delignette-Muller. 2015. A toolbox for nonlinear regression in {R}: The package {nlstools}. J. Stat. Softw. **66**: 1–21.

Chalker, B. E., and D. L. Taylor. 1975. Light-enhanced calcification, and the role of oxidative phosphorylation in calcification of the coral *Acropora cervicornis*. Proc. R. Soc. Lond. B Biol. Sci. **190**: 323–331. doi:10.1098/rspb.1975.0096

Chalker, B. E., and D. L. Taylor. 1978. Rhythmic variations in calcification and photosynthesis associated with the coral *Acropora cervicornis* (Lamarck). Proc. R. Soc. Lond. B Biol. Sci. **201**: 179–189. doi:10.1098/rspb.1978.0039

Chisholm, J. R. 2000. Calcification by crustose coralline algae on the northern Great Barrier Reef, Australia. Limnol. Oceanogr. **45**: 1476–1484. doi:10.4319/lo.2000.45.7.1476

Cohen, I., Z. Dubinsky, and J. Erez. 2016. Light enhanced calcification in hermatypic corals: New insights from light spectral responses. Front. Mar. Sci. **2**: 122. doi:10.3389/fmars.2015.00122

Comeau, S., P. J. Edmunds, N. B. Spindel, and R. C. Carpenter. 2013. The responses of eight coral reef calcifiers to increasing partial pressure of CO_2 do not exhibit a tipping point. Limnol. Oceanogr. **58**: 388–398. doi:10.4319/lo.2013.58.1.0388

Comeau, S., P. J. Edmunds, C. A. Lantz, and R. C. Carpenter. 2014. Water flow modulates the response of coral reef

communities to ocean acidification. Sci. Rep. **4**: 1–6. doi:10.1038/srep06681

Comeau, S., C. E. Cornwall, C. A. Pupier, T. M. DeCarlo, C. Alessi, R. Trehern, and M. T. McCulloch. 2019. Flow-driven micro-scale pH variability affects the physiology of corals and coralline algae under ocean acidification. Sci. Rep. **9**: 1–12. doi:10.1038/s41598-019-49044-w

Cyronak, T., I. R. Santos, and B. D. Eyre. 2013. Permeable coral reef sediment dissolution driven by elevated pCO_2 and pore water advection. Geophys. Res. Lett. **40**: 4876–4881. doi:10.1002/grl.50948

Cyronak, T., and others. 2018. Taking the metabolic pulse of the world's coral reefs. PLoS One **13**: e0190872. doi:10.1371/journal.pone.0190872

Darling, E. S., L. Alvarez-Filip, T. A. Oliver, T. R. Mcclanahan, and I. M. Côté. 2012. Evaluating life-history strategies of reef corals from species traits. Ecol. Lett. **15**: 1378–1386. doi:10.1111/j.1461-0248.2012.01861.x

Diaz-Pulido, G., K. R. N. Anthony, D. I. Kline, S. Dove, and O. Hoegh-Guldberg. 2012. Interactions between ocean acidification and warming on the mortality and dissolution of coralline algae. J. Phycol. **48**: 32–39. doi:10.1111/j.1529-8817.2011.01084.x

Dickson, A. G., C. L. Sabine, and J. R. Christian. 2007. Guide to best practices for ocean CO_2 measurements. Publ, p. 3.

Edmunds, P. J., and others. 2016. Integrating the effects of ocean acidification across functional scales on tropical coral reefs. Bioscience **66**: 350–362. doi:10.1093/biosci/biw023

Edmunds, P. J., G. Tsounis, R. Boulon, and L. Bramanti. 2018. Long-term variation in light intensity on a coral reef. Coral Reefs **37**: 955–965. doi:10.1007/s00338-018-1721-y

Eyre, B. D., A. J. Andersson, and T. Cyronak. 2014. Benthic coral reef calcium carbonate dissolution in an acidifying ocean. Nat. Clim. Chang. **4**: 969–976. doi:10.1038/nclimate2380

Eyre, B. D., T. Cyronak, P. Drupp, E. H. De Carlo, J. P. Sachs, and A. J. Andersson. 2018. Coral reefs will transition to net dissolving before end of century. Science **359**: 908–911. doi:10.1126/science.aao1118

Falkowski, P. G., Z. Dubinsky, L. Muscatine, and J. W. Porter. 1984. Light and the bioenergetics of a symbiotic coral. Bioscience **34**: 705–709. doi:10.2307/1309663

Furla, P., I. Galgani, I. Durand, and D. Allemand. 2000. Sources and mechanisms of inorganic carbon transport for coral calcification and photosynthesis. J. Exp. Biol. **203**: 3445–3457.

Gattuso, J.-P., M. Frankignoulle, S. V. Smith, and O. Océ. 1999. Measurement of community metabolism and significance in the coral reef CO_2 source-sink debate.

Gattuso, J.-P., S. Reynaud-Vaganay, P. Furla, S. Romaine-Lioud, J. Jaubert, I. Bourge, and M. Frankignoulle. 2000. Calcification does not stimulate photosynthesis in the zooxanthellate scleractinian coral Stylophora pistillata. Limnol. Oceanogr. **45**: 246–250. doi:10.4319/lo.2000.45.1.0246

González-Barrios, F. J., and L. Álvarez-Filip. 2018. A framework for measuring coral species-specific contribution to reef functioning in the Caribbean. Ecol. Indic. **95**: 877–886. doi:10.1016/J.ECOLIND.2018.08.038

Goreau, T. F. 1959. The physiology of skeleton formation in corals. A method for measuring the rate of calcium deposition by corals under different conditions. Biol. Bull. **116**: 59–75. doi:10.2307/1539156

Green, D. H. D., P. P. J. Edmunds, and R. R. C. Carpenter. 2008. Increasing relative abundance of *Porites astreoides* on Caribbean reefs mediated by an overall decline in coral cover. Mar. Ecol. Prog. Ser. **359**: 1–10. doi:10.3354/meps07454

Harianto, J., N. Carey, and M. Byrne. 2019. respR—An R package for the manipulation and analysis of respirometry data. Methods Ecol. Evol. **10**: 912–920. doi:10.1111/2041-210X.13162

Heyward, A. J., and A. P. Negri. 1999. Natural inducers for coral larval metamorphosis. Coral Reefs **18**: 273–279. doi:10.1007/s003380050193

Hoegh-Guldberg, O., L. Pendleton, and A. Kaup. 2019. People and the changing nature of coral reefs. Reg. Stud. Mar. Sci. **30**: 100699. doi:10.1016/j.rsma.2019.100699

Hughes, T. P. 1987. Skeletal density and growth form of corals.

Hughes, T. P., and others. 2018. Global warming transforms coral reef assemblages. Nature **556**: 492–496. doi:10.1038/s41586-018-0041-2

Jackson, J., M. Donovan, K. Cramer, and V. Lam. 2014. Status and trends of Caribbean coral reefs: 1970–2012, Global Coral Reef Monitoring Network. IUCN.

Jassby, A. D., and T. Platt. 1976. Mathematical formulation of the relationship between photosynthesis and light for phytoplankton. Limnol. Oceanogr. **21**: 540–547. doi:10.4319/lo.1976.21.4.0540

Jokiel, P. L. 1978. Effects of water motion on reef corals. **35**: 87–97. doi:10.1016/0022-0981(78)90092-8

Kleypas, J., and K. Yates. 2009. Coral reefs and ocean acidification. Oceanography **22**: 108–117. doi:10.5670/oceanog.2009.101

Kornder, N. A., B. M. Riegl, and J. Figueiredo. 2018. Thresholds and drivers of coral calcification responses to climate change. Glob. Chang. Biol. **24**: 5084–5095. doi:10.1111/gcb.14431

Kuffner, I. B., E. Bartels, A. Stathakopoulos, I. C. Enochs, G. Kolodziej, L. T. Toth, and D. P. Manzello. 2017. Plasticity in skeletal characteristics of nursery-raised staghorn coral, *Acropora cervicornis*. Coral Reefs **36**: 679–684. doi:10.1007/s00338-017-1560-2

Kuffner, I. B., L. T. Toth, J. H. Hudson, W. B. Goodwin, A. Stathakopoulos, L. A. Bartlett, and E. M. Whitcher. 2019. Improving estimates of coral reef construction and erosion with in situ measurements. Limnol. Oceanogr. **64**: 2283–2294. doi:10.1002/LNO.11184

Lirman, D. 2000. Fragmentation in the branching coral *Acropora palmata* (Lamarck): Growth, survivorship, and reproduction of colonies and fragments. J. Exp. Mar. Biol. Ecol. **251**: 41–57. doi:10.1016/S0022-0981(00)00205-7

Littler, M. M., and D. S. Littler. 2013. The nature of crustose coralline algae and their interactions on reefs. Research and discoveries: the revolution of science through SCUBA. Smithsonian Institution, Washington, District of Columbia 20013- 7012, USA.

Long, M. H., P. Berg, D. de Beer, J. C. Zieman, D. de Beer, and J. C. Zieman. 2013. In situ coral reef oxygen metabolism: An Eddy correlation study. PLoS One **8**: e58581. doi:10.1371/journal.pone.0058581

Marsh, J. A., and S. V. Smith. 1978. Productivity measurements of coral reefs in flowing water. 361–377.

McConnaughey, T. A., and J. F. Whelan. 1997. Calcification generates protons for nutrient and bicarbonate uptake. Earth Sci. Rev. **42**: 95–117. doi:10.1016/S0012-8252(96)00036-0

Muehllehner, N., C. Langdon, A. Venti, and D. Kadko. 2016. Dynamics of carbonate chemistry, production, and calcification of the Florida Reef Tract (2009-2010): Evidence for seasonal dissolution. Global Biogeochem. Cycles **30**: 661–688. doi:10.1002/2015GB005327

Perry, C. T., and L. Alvarez-Filip. 2018. Changing geo-ecological functions of coral reefs in the Anthropocene. Blackwell Publishing Ltd.

Precht, W. F., A. W. Bruckner, R. B. Aronson, and R. J. Bruckner. 2002. Endangered acroporid corals of the Caribbean. Coral Reefs **21**: 41–42. doi:10.1007/s00338-001-0209-2

Rodríguez-Martínez, R. E., A. T. Banaszak, M. D. McField, A. U. Beltrán-Torres, and L. Álvarez-Filip. 2014. Assessment of *Acropora palmata* in the mesoamerican reef system. PLoS One **9**: 1–7. doi:10.1371/journal.pone.0096140

R Core Team. 2019. R: A language and environment for statistical computing.

Sawall, Y., E. J. Hochberg, Y. Sawall Id, and E. J. Hochberg. 2018. Diel versus time-integrated (daily) photosynthesis and irradiance relationships of coral reef organisms and communities. PLoS One **13**: e0208607. doi:10.1371/journal.pone.0208607

Schneider, C. A., W. S. Rasband, and K. W. Eliceiri. 2012. NIH image to ImageJ: 25 years of image analysis. Nat. Methods **9**: 671–675. doi:10.1038/nmeth.2089

Smith, S. V., and D. W. Kinsey. 1978. Calcification and organic carbon metabolism as indicated by carbon dioxide, p. 469–484. *In* D. R. Stoddart and R. E. Johannes [eds.]. Coral Reefs: Research Methods. UNESCO.

Sorek, M., E. M. Díaz-Almeyda, M. Medina, and O. Levy. 2014. Circadian clocks in symbiotic corals: The duet between Symbiodinium algae and their coral host. Mar. Genomics **14**: 47–57. doi:10.1016/j.margen.2014.01.003

Suggett, D. J., L. F. Dong, T. Lawson, E. Lawrenz, L. Torres, and D. J. Smith. 2013. Light availability determines susceptibility of reef building corals to ocean acidification. Coral Reefs **32**: 327–337. doi:10.1007/s00338-012-0996-7

Takeshita, Y., T. Cyronak, T. R. Martz, T. Kindeberg, and A. J. Andersson. 2018. Coral reef carbonate chemistry variability at different functional scales. Front. Mar. Sci. **5**: 175. doi:10.3389/fmars.2018.00175

Takeshita, Y., W. McGillis, E. M. Briggs, A. L. Carter, E. M. Donham, T. R. Martz, N. N. Price, and J. E. Smith. 2016. Assessment of net community production and calcification of a coral reef using a boundary layer approach. J. Geophys. Res. Ocean **121**: 5655–5671. doi:10.1002/2016JC011886

Toth, L. T., A. Stathakopoulos, I. B. Kuffner, R. R. Ruzicka, M. A. Colella, and E. A. Shinn. 2019. The unprecedented loss of Florida's reef-building corals and the emergence of a novel coral-reef assemblage. Ecology **100**: e02781. doi:10.1002/ECY.2781

Tunnicliffe, V. 1981. Breakage and propagation of the stony coral *Acropora cervicornis*. Proc. Natl. Acad. Sci. **78**: 2427–2431. doi:10.1073/pnas.78.4.2427

Wang, F. 2016. Tutorial SIOX plugin in ImageJ: Area measurement made easy. UV4Plants Bull. **2016**: 37–44. doi:10.19232/uv4pb.2016.2.11

Wickham, H. 2016. ggplot2: Elegant graphics for data analysis. Springer International Publishing,

Wickham, H. 2019. Welcome to the tidyverse. J. Open Source Softw. **4**: 1686.

Yates, K. K., D. G. Zawada, N. A. Smiley, and G. Tiling-Range. 2017. Divergence of seafloor elevation and sea level rise in coral reef ecosystems. Biogeosciences **14**: 1739–1772. doi:10.5194/BG-14-1739-2017

Acknowledgments

This research was funded by the Ocean Acidification program at Mote International Center for Reef Restoration and Research, the Scottish Alliance for Geoscience, Environment, and Society (SAGES), and the University of Glasgow College of Science Student Mobility Award. J.M. thanks the Coral Conservation Society for their additional support. Thanks to the Mote Reef Restoration program for the use of coral fragments and to Dr Heather Page for advice on the incubation methodology at Mote. A special thank you to Mote staff chemists Alexandra Fine and Amanda Quasunella, and to research interns Jill Ashey and Arielle Martinka for their help with conducting incubations and analyzing carbonate chemistry samples. We also thank Dr Patrick Neale for reviewing photosynthesis–irradiance models. Two anonymous reviewers provided insightful comments that improved the manuscript.

Conflict of Interest

None.

Submitted 16 March 2021
Revised 19 November 2021
Accepted 28 November 2021

Associate editor: Steeve Comeau